Ecological Indicators 102 (2019) 801–812

Contents lists available at ScienceDirect

Ecological Indicators

journal homepage: www.elsevier.com/locate/ecolind

Original Articles

Combining hyperspectral imagery and LiDAR pseudo-waveform for predicting crop LAI, canopy height and above-ground biomass

Shezhou Luo[a,*], Cheng Wang[b], Xiaohuan Xi[b], Sheng Nie[b], Xieyu Fan[a], Hanyue Chen[a], Xuebo Yang[b], Dailiang Peng[b], Yi Lin[c], Guoqing Zhou[d]

[a] College of Resources and Environment, Fujian Agriculture and Forestry University, Fuzhou 350002, China
[b] Key Laboratory of Digital Earth Science, Institute of Remote Sensing and Digital Earth, Chinese Academy of Sciences, Beijing 100094, China
[c] Institute of Remote Sensing and Geographic Information Systems, School of Earth and Space Sciences, Peking University, Beijing 100871, China
[d] Guilin University of Technology, Guilin 541004, China

ARTICLE INFO

Keywords:
LiDAR
LAI
Canopy height
Biomass
Pseudo-waveform

ABSTRACT

Crop Leaf area index (LAI), canopy height and above-ground biomass (AGB) are important structural parameters. Accurate predictions of these three parameters are required for improving the applications of crop growth monitoring, health status assessment and yield prediction. Airborne Light Detection and Ranging (LiDAR) system is the most reliable technique for accurately predicting vegetation structure parameters. LiDAR technique has been broadly applied to estimate vegetation LAI, height and biomass, and reliable prediction results have been obtained. However, LiDAR data lack the spectral information of vegetation. The combination of LiDAR data and hyperspectral imagery can achieve complementary advantages of two data sources and improve the prediction accuracies of vegetation parameters. In this research, we aim to estimate maize LAI, canopy height and AGB using the combined hyperspectral imagery and LiDAR pseudo-waveforms. We constructed the LiDAR pseudo-waveforms through discrete-return point clouds and extracted pseudo-waveform variables. The prediction models of maize LAI, canopy height and AGB were established with a random forest (RF) regression algorithm using the traditional statistical variables derived from discrete-return point clouds, the pseudo-waveform variables, the combined hyperspectral vegetation indices and pseudo-waveform variables, respectively. Moreover, the comparative analyses of the three prediction models were conducted to determine the optimal prediction model and explore the potential of the combined hyperspectral vegetation indices and pseudo-waveform variables for predicting maize crop structural parameters. The results showed the strong relationships between LiDAR pseudo-waveform variables and maize LAI, height, and biomass (R^2 = 0.799, 0.832 and 0.871, respectively). Moreover, the pseudo-waveform variables produced better results than the results estimated from traditional statistical variables of discrete-return LiDAR (R^2 = 0.772, 0.812 and 0.811, respectively). Therefore, it is a viable method for predicting maize LAI, canopy height and AGB using the LiDAR pseudo-waveforms created from discrete-return LiDAR data. Nevertheless, we found that the combined pseudo-waveform variables and vegetation indices derived from hyperspectral imagery produced a better prediction result (R^2 = 0.829, 0.892 and 0.909, respectively) when compared to LiDAR pseudo-waveform data alone, and the prediction accuracies improved by 3.8%, 7.2% and 4.4%, respectively. The combined hyperspectral imagery and LiDAR pseudo-waveform data provided complementary information and therefore improved prediction accuracies of these parameters. Although small improvements were observed, the combined data have potential for improving predictions of crop parameters. Our study will provide valuable information for predicting vegetation LAI, canopy height and AGB using the combined hyperspectral imagery and pseudo-waveform constructed from discrete-return LiDAR data.

1. Introduction

Leaf area index (LAI), canopy height and above-ground biomass (AGB) are essential vegetation structure parameters (Chen et al., 1997; Chopping et al., 2008). Accurate predictions of these parameters are very important for improving the applications of crop growth

* Corresponding author.
E-mail address: luoshezhou@163.com (S. Luo).

https://doi.org/10.1016/j.ecolind.2019.03.011
Received 21 November 2018; Received in revised form 26 January 2019; Accepted 8 March 2019
Available online 28 March 2019
1470-160X/

monitoring, health status assessment and yield prediction (Kross et al., 2015). Field observations are the most accurate method for obtaining vegetation LAI, height and biomass. Nevertheless, field observations are time-consuming, costly and labor-intensive (Tao et al., 2014). Moreover, destructive sampling is required sometimes (Moeser et al., 2014). Therefore, field observation method is difficult to obtain vegetation parameters across the landscape, and is often used as effective calibration and validation of other methods (García et al., 2018; Jonckheere et al., 2004).

Remote sensing techniques are able to economically, quickly and repeatedly obtain large-scale land surface information, which have been broadly applied in estimation of vegetation parameter (Chen and Cihlar, 1996; Varvia et al., 2018). Vegetation parameter prediction based on passive optical remote sensing mainly applies the empirical relationships between field-observed vegetation parameter and vegetation index (VI) extracted from remote sensing imagery. Using VIs to estimate vegetation parameters is simple and easy to implement in practice. However, vegetation indices are easily affected by the soil background and atmospheric conditions, and especially in densely vegetated or high biomass areas, the vegetation indices tend to saturate, which will decrease prediction accuracies of vegetation parameters (Karna et al., 2015; Mutanga and Skidmore, 2004). Although microwave remote sensing can partially penetrate vegetation canopy and has a higher saturation level, the saturation problem still limits the applications of microwave remotely sensed data in predicting vegetation parameters (Lu, 2006; Lucas et al., 2006).

Airborne LiDAR systems can rapidly and accurately capture three-dimensional data (Qin et al., 2015). Previous studies showed that LiDAR data can reduce the saturation problem often encountered in optical remotely sensed data (Riaño et al., 2004; Zhao and Popescu, 2009), which have been broadly applied to predict canopy height (Gao et al., 2015; Glenn et al., 2011; Mielcarek et al., 2018; Pang et al., 2011), gap fraction and cover (Anderson et al., 2018; Hopkinson and Chasmer, 2009; Zheng et al., 2017), LAI (Heiskanen et al., 2015; Ma et al., 2014; Richardson et al., 2009) and biomass (Chen, 2015; Dalponte et al., 2018; Li et al., 2015; Ma et al., 2018; Nie et al., 2017; Takagi et al., 2015; Xi et al., 2016). Previous these studies showed that LiDAR data are able to reliably predict vegetation structural parameter and no saturation problem is found.

According to the way of return recording, airborne LiDAR systems are divided into discrete-return LiDAR and full-waveform LiDAR. Discrete-return LiDAR systems only record limited returns, such as first, last and intermediate returns; however, full-waveform LiDAR systems can record the whole laser return energy reflected from the illuminated surfaces and obtain vertical waveform profile of each LiDAR shot (Zolkos et al., 2013). Compared with discrete-return LiDAR, full-waveform LiDAR can reflect the vertical information of vegetation in detail and provide more information of ground objects (Alexander et al., 2015; Fieber et al., 2015; Zhou and Qiu, 2015). Full-waveform LiDAR has been increasingly applied to estimate vegetation structure parameters; nevertheless, only limited large-footprint full-waveform LiDAR data are available today. Therefore, many studies have been carried out using small-footprint full-waveform LiDAR data to synthetize large-footprint pseudo-waveform LiDAR data (Hermosilla et al., 2014; Li et al., 2016; Magruder, 2010; Pirotti et al., 2014). In order to make full use of the information of discrete-return LiDAR data and improve the prediction accuracies of vegetation structural parameters, some researchers applied discrete-return point clouds to simulate pseudo-waveforms (Muss et al., 2011; Popescu and Zhao, 2008). Lovell et al. (2003) showed that intensity values of discrete-return LiDAR could be used to create pseudo-waveform data, and pseudo-waveform data could be less dominated by individual tall trees or missing treetops. Muss et al. (2011) demonstrated that prediction models of forest structure parameters constructed using pseudo-waveform variables performed comparably to or better than using statistical variables of discrete-return LiDAR. Moreover, some previous studies showed that LiDAR pseudo-waveforms created using discrete-return point clouds resemble closely the true observed waveforms (Duncanson et al., 2010; Popescu et al., 2011; Zhou and Qiu, 2015). Silva et al. (2018) compared the performance of simulated waveforms from discrete-return point clouds and large-footprint LiDAR waveforms for forest parameters prediction, and they found that the simulated waveforms and large-footprint LiDAR waveforms had the equivalent prediction performance. Therefore, the pseudo-waveforms created from discrete-return point clouds have potential for predicting vegetation structure parameters. Nevertheless, no studies have been performed on the prediction of crop structure parameters using pseudo-waveforms. Although LiDAR pseudo-waveform can offer accurate vertical information, it lacks the spectral information of vegetation (Zhou and Qiu, 2015). Therefore, the combined pseudo-waveforms and hyperspectral data can make full use of their respective advantages, which will help to improve prediction accuracy of vegetation parameters. Overall, in previous work, the estimates of vegetation structure parameters using pseudo-waveform data mainly concentrated on forest vegetation; however, no researchers explored whether the pseudo-waveform data can be used to estimate the structure parameters of low vegetation. In addition, no studies, to our best knowledge, have been reported to estimate maize crop LAI, canopy height and AGB using LiDAR pseudo-waveforms alone or the combined hyperspectral imagery and pseudo-waveforms.

The purpose of this study is to estimate maize LAI, canopy height and AGB using the combined hyperspectral imagery and LiDAR pseudo-waveforms. We will 1) construct LiDAR pseudo-waveform from discrete-return point clouds and extract LiDAR pseudo-waveform variables; 2) estimate maize LAI, canopy height and AGB applying pseudo-waveform variables alone, and compare with the prediction models created using statistical variables from discrete-return LiDAR data; 3) estimate maize LAI, canopy height and AGB applying the combined hyperspectral imagery and pseudo-waveforms; and 4) assess the prediction accuracies of maize crop LAI, canopy height and AGB.

2. Materials and methods

2.1. Study area and field-measured data

(1) Study area

Our research was carried out in Zhangye City of Gansu Province, China (38°50′N-38°59′N, 100°20′E-100°28′E). The research area is flat with an average altitude of 1403 m. The main crops are maize, wheat and vegetables in this study area. Remotely sensed data were provided by the HiWATER project and Li et al. (2013) gave a detailed description of the project's experimental scheme and data-acquisition parameters.

(2) Field-measured data

Field measurements were conducted on July 13–16, 2012. The plot size was a square with side length of five meters. In each plot, we measured the heights of eleven maize plants using a tape measure, and the total number (n) of maize in the plot were recorded. The average of eleven maize heights (h, m) in the plot was considered to be the field-measured height of the plot. A series of corn plants with different heights were cut at ground level. The height of all plants was measured in the laboratory and then were dried in an oven at 75 °C until constant weight was achieved. The empirical relationship (Eq. (1)) between single plant height and biomass was developed ($R^2 = 0.95$, RMSE = 15.8 g/plant), and refer to Luo et al. (2016) for more details. And then, the above-ground biomass density (AGB, g/m^2) of each plot was calculated using Eq. (2). The LAI values of all samples were measured by LAI-2200 sensor. The locations of all samples were measured using the RTK-GPS. Finally, we obtained 42 field-measured samples of maize LAI, canopy height and AGB. The ranges of LAI, height and biomass are 1.28–4.69 (mean: 2.75), 1.059–3.091 m (mean: 2.08 m)

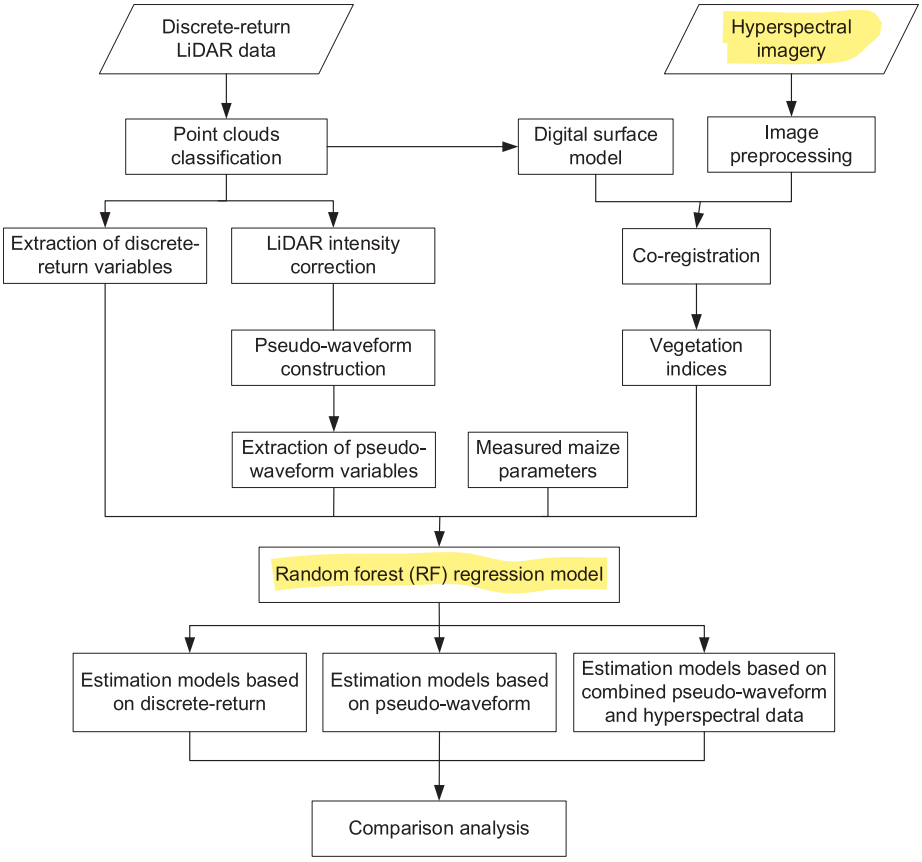

Fig. 1. Methodology flowchart of data processing and estimation of maize LAI, height and biomass.

and 204.83–3039.82 g/m^2 (mean: 1465.49 g/m^2), respectively.

$$b = 129.72 \times h - 131.16 \quad (1)$$

$$AGB = \frac{b \times n}{5 \times 5} \quad (2)$$

2.2. Airborne discrete-return LiDAR data

Discrete-return LiDAR data applied in the research were acquired on July 19, 2012 using Leica ALS70 systems (Xiao and Wen, 2013). The average flight height was 1300 m and flight speed was 60 m/s. The scan angle ranged from −18 to +18°. The laser point density in this study area was 7.32 points/m^2, and the post spacing was 0.37 m. Raw laser points include three-dimensional coordinates and return intensity. LiDAR point clouds were classified using TerraSolid software. Moreover, digital surface model (DSM) with one-meter resolution was generated using the classified LiDAR data. Fig. 1 shows the methodology flowchart for estimating maize LAI, height and biomass in this study.

LiDAR intensity values are related to the energy emitted by LiDAR sensor, the atmosphere and the distance between sensor and target. LiDAR intensity values may be different for the same type of objects due to different data-acquisition environment. Therefore, LiDAR intensity data should be corrected and normalized before they are applied. Since the atmospheric conditions were the same for the LiDAR data acquisition, this study only considered the influence of the incident angle and the range from the laser scanner to the target on the LiDAR intensity. The original intensity values were corrected using Eq. (3) (Mesas-Carrascosa et al., 2012).

$$I_{corrected} = I \times \frac{R^2}{R_s^2 \cos \alpha} \quad (3)$$

where $I_{corrected}$ and I are the corrected and raw intensity value, respectively; R is the sensor to target range; R_s is the reference range, and α is the incident angle.

2.2.1. LiDAR pseudo-waveforms construction

In this study, LiDAR pseudo-waveforms were constructed using intensity values and return count of discrete-return LiDAR data, respectively. The construction method of pseudo-waveform consisted of the following four steps:

(1) LiDAR point clouds in each plot were sorted by elevation values and assigned to the corresponding height bins at height interval of 0.15 m.
(2) Counted the return intensity and return count in each height bin, respectively.
(3) Calculated the relative return count or intensity in each height bin by dividing the return count or sum of intensity in each height bin by the total return count or total intensity.
(4) LiDAR pseudo-waveform was constructed when the relative return intensity or return count corresponding to the elevation of each height bin was connected with a smooth curve (Fig. 2).

For each field plot, laser points were extracted using a circle with a radius of 3 m around the plot center. Finally, a total of 42 pseudo-waveforms were constructed according to the method described above.

2.2.2. Extraction of LiDAR pseudo-waveform variables

To obtain accurate waveform variables, in this research we used a Gaussian decomposition method to decompose every LiDAR pseudo-waveform into multiple Gaussian functions (Wagner et al., 2006). As shown in Fig. 3, intensity-based pseudo-waveform was decomposed into three Gaussian components. The last Gaussian component is assumed to the ground signal and represent the ground elevation (Duong

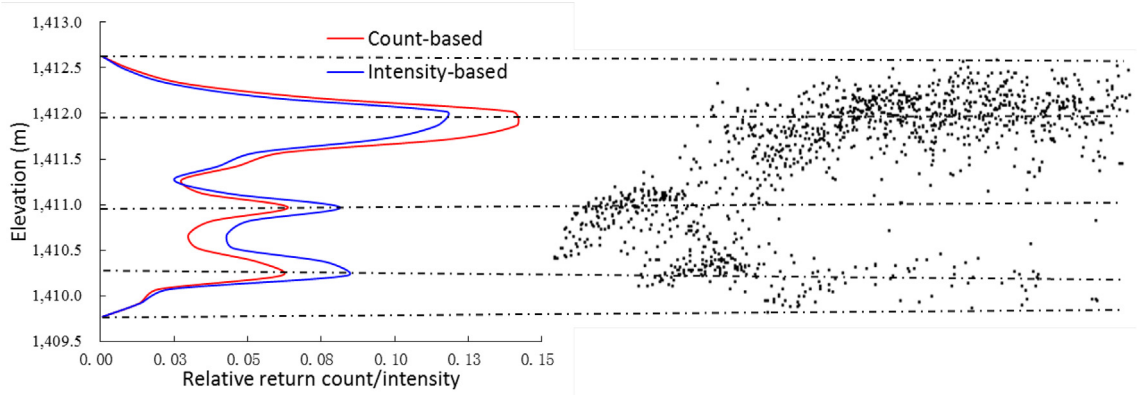

Fig. 2. The distribution of LiDAR point clouds of a maize canopy and the corresponding LiDAR pseudo-waveform. Blue curve and red curve are intensity- and count-based LiDAR pseudo-waveforms.

et al., 2008; Tian et al., 2015). Based on the decomposed waveform, we extracted a series of waveform variables (Table 1) using to estimate maize LAI, height and biomass. These variables mainly include canopy height variables and fractional cover variables. Canopy return ratio (CRR) variable is used to describe the fractional cover, which was calculated by dividing the sum of canopy intensity by the total intensity of the pseudo-waveform. Height of median energy (HOME) is an important waveform variable for predicting vegetation parameter (Clark et al., 2011; Drake et al., 2003).

2.2.3. Variables from discrete-return LiDAR

Commonly used variables to predict vegetation parameters are statistical variables calculated from discrete-return LiDAR. To compare the prediction models constructed from LiDAR pseudo-waveform variables with the models constructed from discrete-return point clouds, we calculated a series of statistical variables based on discrete-return point clouds (Table 2)

2.3. Hyperspectral imagery and processing

Hyperspectral imagery was acquired by CASI sensor (ITRES Research Ltd., Calgary, Alberta, Canada) on June 29, 2012. The data had 48 bands with one-meter resolution. Table 3 shows the data-acquisition parameters in this research. Hyperspectral CASI data were atmospherically corrected by the FLAASH method (www.exelisvis.com). The CASI imagery was manually co-registered using the DSM generated from LiDAR data with a registration error less than 1 pixel (< 1 m).

Vegetation indices (VIs) derived from passive optical remotely sensed imagery are broadly applied to estimate vegetation LAI, height and biomass through an empirical model between VIs and field-measured values. The narrow-band VIs have been increasingly applied to predict vegetation parameters. Compared to broad-band VIs, narrow-band VIs are able to decrease the influence of signal saturation and have potential for improving prediction accuracies of vegetation parameters. The narrow-band VIs applied in this research are shown in Table 4, and ρ is the reflectivity.

2.4. Prediction of maize crop structural parameters

Maize LAI, height and biomass were estimated using pseudo-waveform variables, statistical variables calculated from discrete-return point clouds, and the combined VIs and pseudo-waveform variables, respectively. Moreover, the comparative analyses of the three prediction models were performed to determine the optimal prediction model and explore the potential of the combined data for predicting maize structure parameters. In this research, we applied a random forest (RF) regression model to estimate maize LAI, height and biomass. RF is a non-parametric statistical approach that can be used for both regression and classification (Gleason and Im, 2012). In RF regression, the out-of-bag data are used to assess model performance, which can avoid the need for independent validation (Breiman, 2001). To establish prediction models of LAI, height and biomass, RF regression analysis was performed using the RF package (Liaw and Wiener, 2002) in R statistical software. The predictive powers of prediction models of maize LAI, canopy height and AGB were assessed through coefficient of

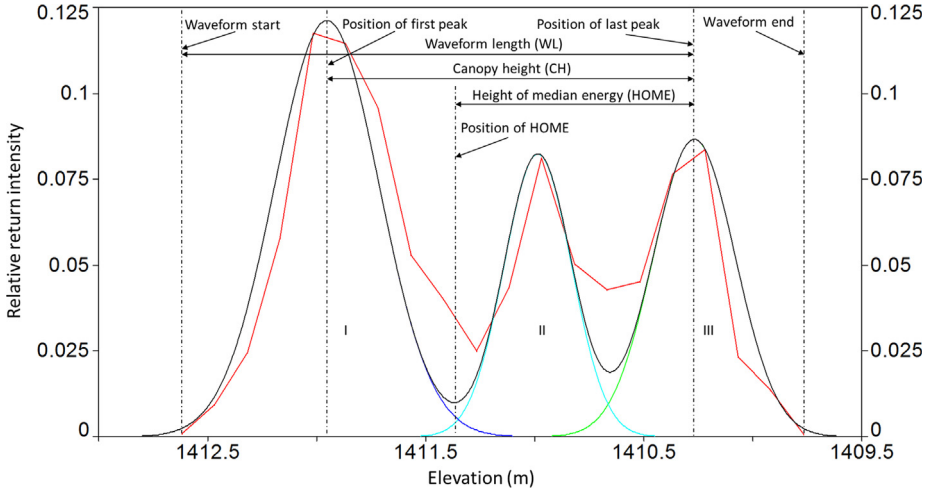

Fig. 3. Raw LiDAR pseudo-waveform (in red), fitted curve (in black) and three decomposed Gaussian components (I, II, III).

Table 1
LiDAR pseudo-waveform variables.

Variable	Definition
HOME	Height of median energy (HOME) is the height of half the pseudo-waveform energy
CRR	CRR is the ratio of the sum of intensity of all canopy returns to the total intensity of the pseudo-waveform
GRR	The ratio of the sum of intensity of ground returns to the sum of intensity of canopy returns of the pseudo-waveform
CH	The distance between the center of the first Gaussian curve and the center of the last Gaussian curve
WL	The distance between the waveform start and the center of the last Gaussian curve
HOME/WL	HOME divided by WL
WS	The distance between the waveform start and the waveform end
HP	The distance between the locations where the energy is half of the pseudo-waveform energy and the waveform end
FP	The distance between the center of the first Gaussian curve and the waveform end
LP	The distance between the center of the last Gaussian curve and the waveform end

Table 2
Statistical variables calculated using discrete-return point clouds.

Variables	Description
max	Height maximum of point clouds
mean	Height mean of point clouds
sd	Height Standard deviation of point clouds
cv	Height coefficient of variation of point clouds
P (40, 50, 60, 70, 80, 90, 99)	Height percentile of point clouds
LII	Laser intercept index – a descriptor of fractional cover (canopy returns/total returns)

Table 3
Hyperspectral CASI data-acquisition parameters.

Parameters	Specifications
Flight height	2000 m
Swath width	1500 m
Number of bands	48
Spatial resolution	1.0 m
Spectral resolution	7.2 nm
Field of view	40°
Spectral range	380–1050 nm

determination (R^2), root mean squared error (RMSE) and relative RMSE (RMSE%) (Eq. (4)).

$$RMSE\% = \frac{RMSE}{\bar{y}} \quad (4)$$

where $\bar{y}$ is the mean value of the field observations.

3. Results

3.1. LiDAR pseudo-waveform construction

The blue curve and red curve in Fig. 2 were intensity- and count-based LiDAR pseudo-waveforms, respectively. We found that the pseudo-waveforms derived from intensity values and return count were almost the same. However, the pseudo-waveforms constructed from LiDAR intensity data more closely resembled the waveform of large footprint LiDAR (Popescu and Zhao, 2008). Therefore, only intensity-based LiDAR pseudo-waveforms were applied to estimate LAI, height and biomass in our study.

As shown in Fig. 2, we could observe the vertical distribution of maize height from LiDAR point clouds, which was mainly composed of three layers points corresponding to three curves. Moreover, there were three curve peaks in the pseudo-waveform, and the positions were about at 1411.9 m (tall maize), 1411.0 m (short maize) and 1410.3 m (ground), respectively, as illustrated in Fig. 2. Therefore, LiDAR pseudo-waveform was able to reliably reflect vertical profile information of vegetation.

3.2. Prediction of LAI, height and biomass using LiDAR data alone

3.2.1. Variable importance using LiDAR variables alone

The RF regression provided the information of variable importance. Fig. 4 indicates variable importance for predicting maize LAI, canopy height and AGB based on RF regression model. We found that variable importance was different for predicting maize LAI, canopy height and AGB. The most important variables for predicting maize LAI, canopy height and AGB using LiDAR pseudo-waveform variables alone were CRR, HP and HP, respectively.

Fig. 5 shows variable importance for predicting maize LAI, canopy height and AGB using traditional statistical variables, and the most important variables were LII, mean and mean, respectively. Similarly, we found that variable importance was different for predicting maize LAI, height and biomass using statistical variables calculated from discrete-return point clouds. As shown in Figs. 3(a) and 4(a), the best variables for predicting LAI were CRR and LII, which both were metrics used to describe canopy fractional cover.

3.2.2. Prediction results using LiDAR variables alone

Maize LAI, height and biomass predictive models were established based on RF regression using 42 training samples, and summaries of the

Table 4
Narrow-band VIs and equations applied in our research.

Vegetation Index	Equations	References
Normalized difference vegetation index (NDVI)	$(\rho_{797.7} - \rho_{669.1})/(\rho_{797.7} + \rho_{669.1})$	Rouse et al. (1973)
Modified Normalized difference vegetation index (MNDVI)	$(\rho_{754.9} - \rho_{740.6})/(\rho_{754.9} + \rho_{740.6})$	Mutanga and Skidmore (2004)
Simple ratio vegetation index (SRVI1)	$\rho_{797.7}/\rho_{669.1}$	Jordan (1969)
Simple ratio vegetation index (SRVI2)	$\rho_{754.9}/\rho_{712}$	Mutanga and Skidmore (2004)
Atmospherically resistant vegetation index (ARVI)	$(\rho_{797.7} - 2\rho_{669.1} + \rho_{454.4})/(\rho_{797.7} + 2\rho_{669.1} - \rho_{454.4})$	Kaufman and Tanre (1992)
Soil-adjusted vegetation index (SAVI)	$(1 + 0.5)(\rho_{797.7} - \rho_{669.1})/(\rho_{797.7} + \rho_{669.1} + 0.5)$	Huete et al. (1994)
Optimization of soil-adjusted vegetation index (OSAVI)	$(1 + 0.16)(\rho_{797.7} - \rho_{669.1})/(\rho_{797.7} + \rho_{669.1} + 0.16)$	Rondeaux et al. (1996)
Modified soil-adjusted vegetation index (MSAVI)	$0.5 \times (2\rho_{nir} + 1 - \sqrt{(2\rho_{nir} + 1)^2 - 8(\rho_{nir} - \rho_{red})})$	Qi et al. (1994)
Enhanced vegetation index (EVI)	$2.5 \times (\rho_{797.7} - \rho_{669.1})/(\rho_{797.7} + 6\rho_{669.1} - 7.5\rho_{454.4} + 1)$	Huete et al. (1994)

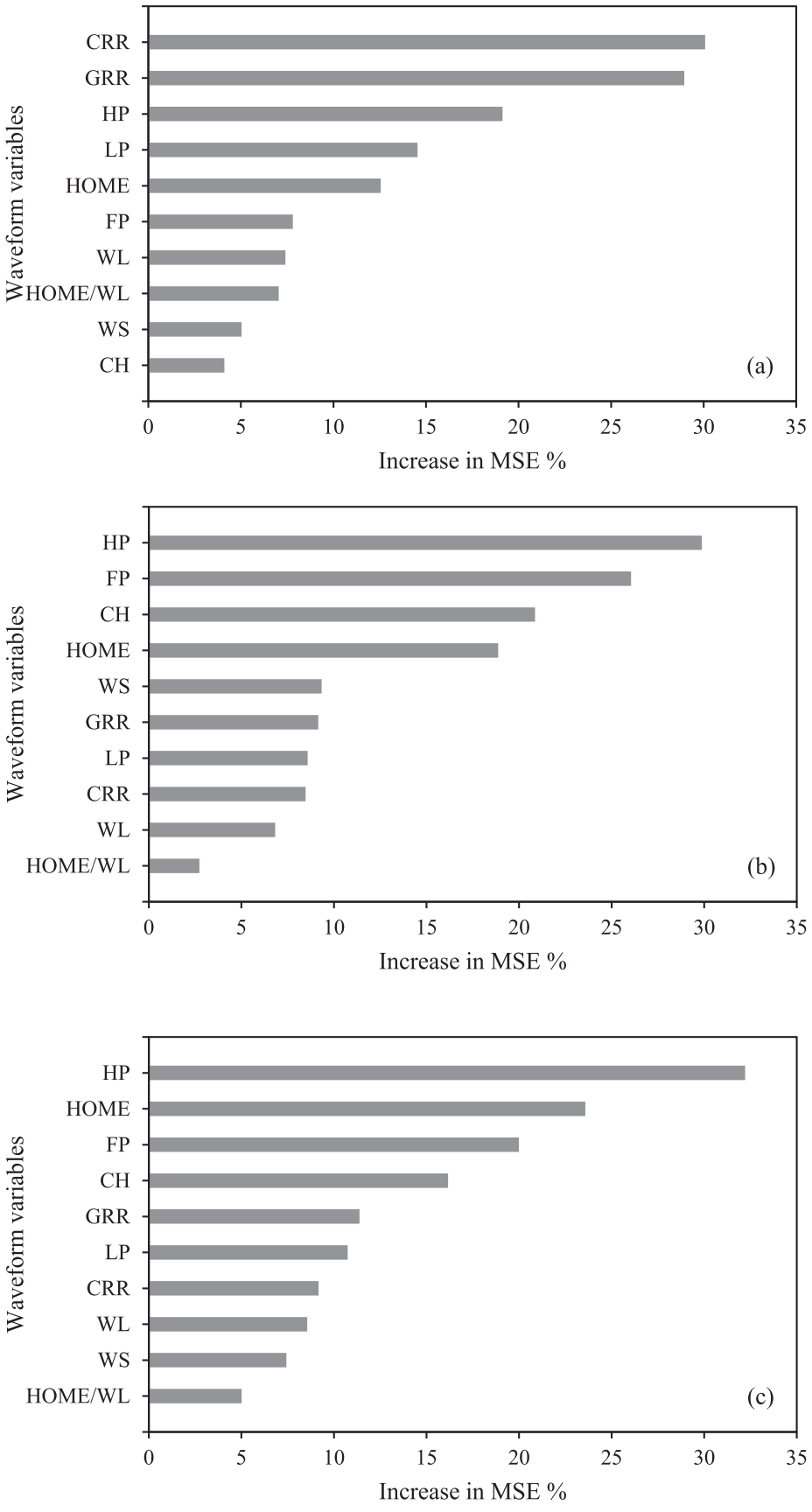

Fig. 4. Variable importance for predicting maize LAI (a), height (b) and biomass (c) by RF regression model using LiDAR pseudo-waveform variables alone.

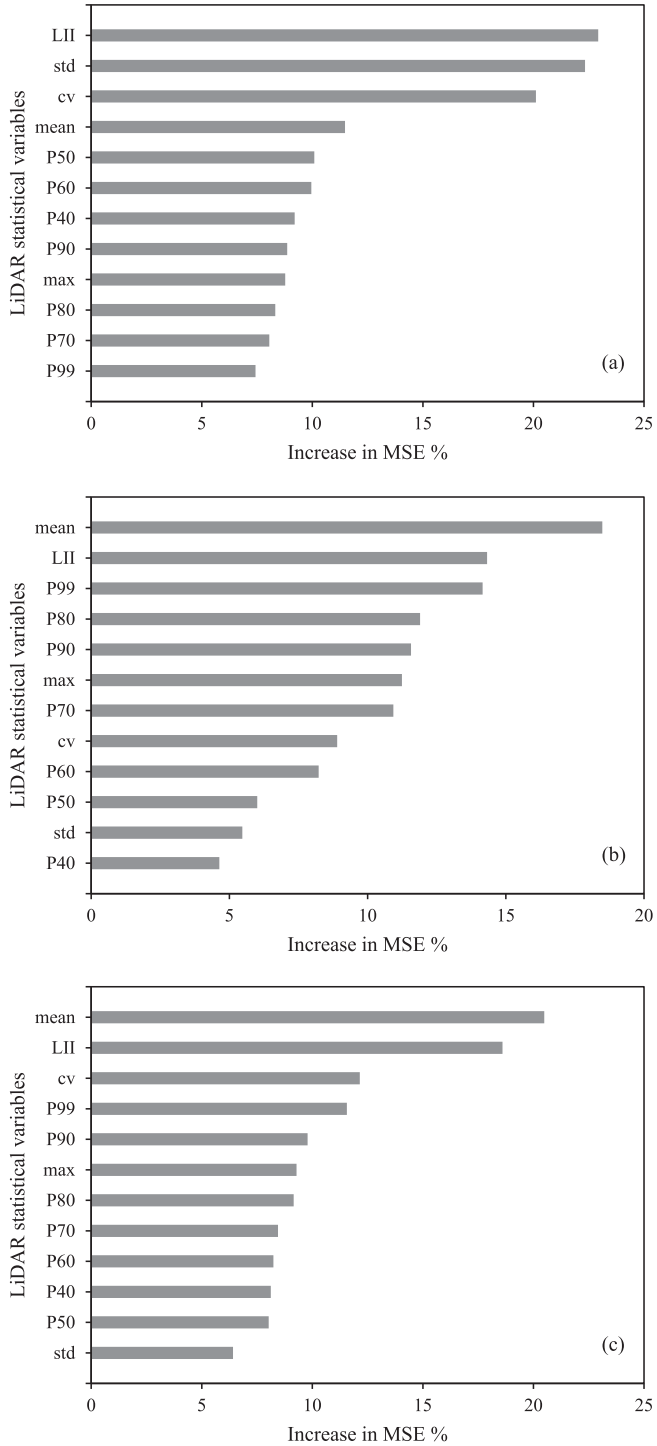

Fig. 5. Variable importance for predicting maize LAI (a), height (b) and biomass (c) by RF regression model using traditional statistical variables derived from discrete-return LiDAR data.

predictive models were shown in Table 5. For pseudo-waveform variables alone, the R^2 values for predicting maize LAI, canopy height and AGB were 0.799 (RMSE = 0.368), 0.832 (RMSE = 0.225 m) and 0.871 (RMSE = 276.1 g/m^2), respectively. Therefore, LiDAR pseudo-waveforms derived from discrete-return point clouds could reliably predict maize LAI, canopy height and AGB. We found that the pseudo-waveform variables had a better predictive performance when compared to the results derived from statistical variables of discrete-return LiDAR (R^2 = 0.772, 0.812 and 0.811, respectively).

3.3. Prediction of LAI, height and biomass using combined hyperspectral and LiDAR pseudo-waveform variables

3.3.1. Variable importance using combined hyperspectral and pseudo-waveform variables

Fig. 6 shows variable importance for predicting maize structure parameters by RF regression algorithm using combined VIs and LiDAR pseudo-waveform variables. The most important variables for predicting maize LAI, canopy height and AGB were CRR, HP and HP, respectively, which were the same as LiDAR pseudo-waveform variables alone. Compared to LiDAR pseudo-waveform variables, the VIs derived from hyperspectral imagery had lower variable importance for predicting maize LAI, height and biomass (Fig. 6). As shown in Fig. 6, the first ten variables for predicting LAI, height and biomass only included one, two and one VIs, respectively. However, some VIs had greater variable importance than some LiDAR pseudo-waveform variables.

3.3.2. Prediction results using combined hyperspectral and pseudo-waveform variables

Summaries of the predictive models of LAI, height and biomass based on combined hyperspectral and pseudo-waveform variables were listed in Table 5. Fig. 7 indicates the scatterplots of field-observed versus predicted maize structure parameters based on RF regression algorithm. Compared to LiDAR pseudo-waveform variables alone, the combined hyperspectral and pseudo-waveform variables provided better prediction accuracies of LAI, canopy height and AGB (R^2 = 0.829, 0.892 and 0.909, respectively), and the R^2 values improved by 3.8%, 7.2% and 4.4% (RMSE decreased by 2.8%, 12.0% and 9.5%), respectively. The improvements of prediction accuracies could be attributed to the complementary information of hyperspectral imagery and LiDAR data. Nevertheless, the combined hyperspectral and pseudo-waveform variables did not significantly improve prediction accuracies of LAI, canopy height and AGB. This might be due to the fact that LiDAR pseudo-waveform variables alone could produce high prediction accuracy of LAI, canopy height and AGB, and therefore, additional hyperspectral information made little contribution to prediction accuracies of LAI, canopy height and AGB.

4. Discussion

In this study, maize LAI, canopy height and AGB were predicted using pseudo-waveform variables, traditional statistical variables from discrete-return LiDAR data and combined hyperspectral and LiDAR pseudo-waveform variables, respectively. Our results suggest that LiDAR pseudo-waveform alone was able to accurately estimate maize LAI, canopy height and AGB. Moreover, the combined hyperspectral imagery and LiDAR pseudo-waveform data improved the prediction accuracies of maize LAI, canopy height and AGB.

4.1. Variable importance for predicting LAI, canopy height and AGB

The RF regression yielded variable importance for all predictor variables. The results showed that the canopy return ratio (CRR) derived from LiDAR pseudo-waveform and laser intercept index (LII) calculated from discrete-return point clouds were the most variable for LAI prediction. Similar results were also obtained in previous studies where they found that canopy cover or canopy gap fraction derived from LiDAR data was the best predictor variable for LAI prediction (Heiskanen et al., 2015; Luo et al., 2018). Using the pseudo-waveform variables to estimate height and biomass, the HP (the range between the location of pseudo-waveform median energy and the waveform end) was the best predictor. However, previous studies showed that HOME was the optimal predictor for predicting biomass (Drake et al., 2002). This may be due to two factors. One was different vegetation types. The other was different LiDAR waveform. In this study, LiDAR waveform data were pseudo-waveforms created from discrete-return

Table 5
Model summaries for predicting maize LAI, height and biomass using pseudo-waveform variables, statistical variables derived from discrete-return LiDAR data and combined VIs and pseudo-waveform variables based on RF regression.

Maize parameter	Variable	R^2	RMSE	RMSE%
LAI	LiDAR statistical variables*	0.772	0.397	14.3
	Pseudo-waveform variables	0.799	0.368	13.3
	Pseudo-waveform variables + VIs	0.829	0.333	12.0
Height	LiDAR Statistical variables*	0.812	0.238 (m)	11.4
	Pseudo-waveform variables	0.832	0.225 (m)	10.8
	Pseudo-waveform variables + VIs	0.892	0.198 (m)	9.5
Biomass	LiDAR Statistical variables*	0.811	335.1 (g/m^2)	22.9
	Pseudo-waveform variables	0.871	276.1 (g/m^2)	18.8
	Pseudo-waveform variables + VIs	0.909	268.3 (g/m^2)	18.3

* LiDAR statistical variables are the variables derived from discrete-return LiDAR data.

LiDAR data, which were not true waveform data like Geoscience Laser Altimeter System (GLAS) waveform data. The true waveform data were successfully applied to estimate vegetation parameters (Ahmed et al., 2013; Nie et al., 2015). In general, variable importance was different for predicting maize LAI, canopy height and AGB. As a consequence, to improve prediction accuracies of vegetation parameters, the suitable predictors should be determined according to the specific vegetation types, vegetation parameters, study area and remotely sensed data.

As shown in Fig. 6, LiDAR pseudo-waveform variables had far greater importance than VIs derived from hyperspectral imagery. For the combined data, the first ten variables for predicting LAI, height and biomass only included one, two and one VIs, respectively. Compared to LiDAR pseudo-waveform variables, VIs made little contribution to the estimation of LAI, height and biomass. Therefore, LiDAR data have more advantage over passive remote sensing data for predicting vegetation structure parameters. This is because laser pulses emitted from LiDAR systems can penetrate the vegetation canopy to ground and produce accurate three-dimensional structural information, which can reduce saturation problem of passive remotely sensed data (Cao et al., 2014; Karna et al., 2015). As a result, LiDAR technology is being increasingly applied to predict vegetation parameters.

4.2. Prediction of LAI, height and biomass using LiDAR variables alone

In this study, we estimated maize structural parameter using LiDAR pseudo-waveform variables and the results indicated that pseudo-waveform variables alone can accurately predict maize LAI, height and biomass (R^2 = 0.799, 0.832 and 0.871, respectively). Our findings were in agreement with previous studies, which demonstrated that LiDAR pseudo-waveform constructed from discrete-return point clouds can accurately predict vegetation parameters (Muss et al., 2011; Popescu and Zhao, 2008). Moreover, the pseudo-waveform variables had a better predictive performance when compared to the results derived from statistical variables of discrete-return LiDAR (R^2 = 0.772, 0.812 and 0.811, respectively), although the improvements of estimation accuracies were not significant. Previous studies also showed that the prediction models based on pseudo-waveform variables were comparable to or better than the models based on traditional statistical variables (Muss et al., 2011). Our results further support the findings. Most previous researchers used the statistical variables extracted from LiDAR data to estimate vegetation structure parameters (e.g., maximum, mean, percentiles, standard deviation of LiDAR height) (Jakubowski et al., 2013; Tesfamichael et al., 2018; Zhao et al., 2012). Although these previous researchers successfully estimated vegetation structural parameters using statistical variables of LiDAR data, the statistical variables cannot be representative of canopy vertical distribution information. Moreover, multiple statistical variables derived from LiDAR data may be highly correlated, which will cause multicollinearity of prediction models. Nevertheless, pseudo-waveform variables can reflect the vertical distribution information of a canopy and have lower correlation among variables. Meanwhile, waveform-based prediction model is more plausible. Therefore, the pseudo-waveforms derived from discrete-return LiDAR data have potential for predicting vegetation structure parameters.

4.3. Prediction of LAI, canopy height and AGB using combined hyperspectral and pseudo-waveform variables

We successfully estimated maize LAI, canopy height and AGB applying the combined hyperspectral imagery and pseudo-waveforms, and the R^2 values were 0.829, 0.892 and 0.909, respectively (Table 5). Compared to LiDAR pseudo-waveforms alone, the combined data improved prediction accuracies of maize LAI, canopy height and AGB (improved by 3.8%, 7.2% and 4.4%, respectively). These improvements can be attributed to the fact that additional hyperspectral data provided complementary information of LiDAR data. Although no research explored the potential for predicting maize LAI, height and biomass using the combined hyperspectral imagery and LiDAR pseudo-waveforms, some studies for predicting forest biomass have been carried out using the combined hyperspectral/multispectral imagery and discrete-return LiDAR data (Laurin et al., 2014; Lucas et al., 2008; Phua et al., 2017). These previous studies showed that the combined LiDAR and hyperspectral/multispectral data could improve prediction accuracies of vegetation biomass when compared to LiDAR data or hyperspectral/multispectral imagery alone. However, the improvement of prediction accuracy in this study was not significant. Similar findings were reported by previous studies, where they found that the combined LiDAR and hyperspectral/multispectral data made a small improvement in prediction accuracy (Laurin et al., 2014; Luo et al., 2017; Swatantran et al., 2011). The reason is that the single LiDAR data had a strong relationship with vegetation structural parameters, and complementary spectral information made a minor contribution to prediction accuracies of vegetation structural parameters. Therefore, LiDAR data are a better data source for predicting vegetation structural parameters. Fig. 8 shows residuals of the predicted maize structure parameters using the combined hyperspectral and LiDAR pseudo-waveform variables. We found that the residuals were affected by the values of maize structural parameters. Overall, the residuals were negatively correlated with maize structural parameters, i.e., the residuals decreased as the values of maize structural parameters increased, particularly for maize height and biomass.

Out results show that it is a viable method for predicting maize LAI, canopy height and AGB applying pseudo-waveform created from discrete-return LiDAR data. The combined hyperspectral imagery and LiDAR pseudo-waveform can produce complementary information for predicting vegetation structural parameters and have potential for improving prediction accuracies of vegetation structural parameters. This research can provide valuable guidance for predicting vegetation structural parameters using the LiDAR pseudo-waveforms constructed from discrete-return point clouds or the combined LiDAR pseudo-

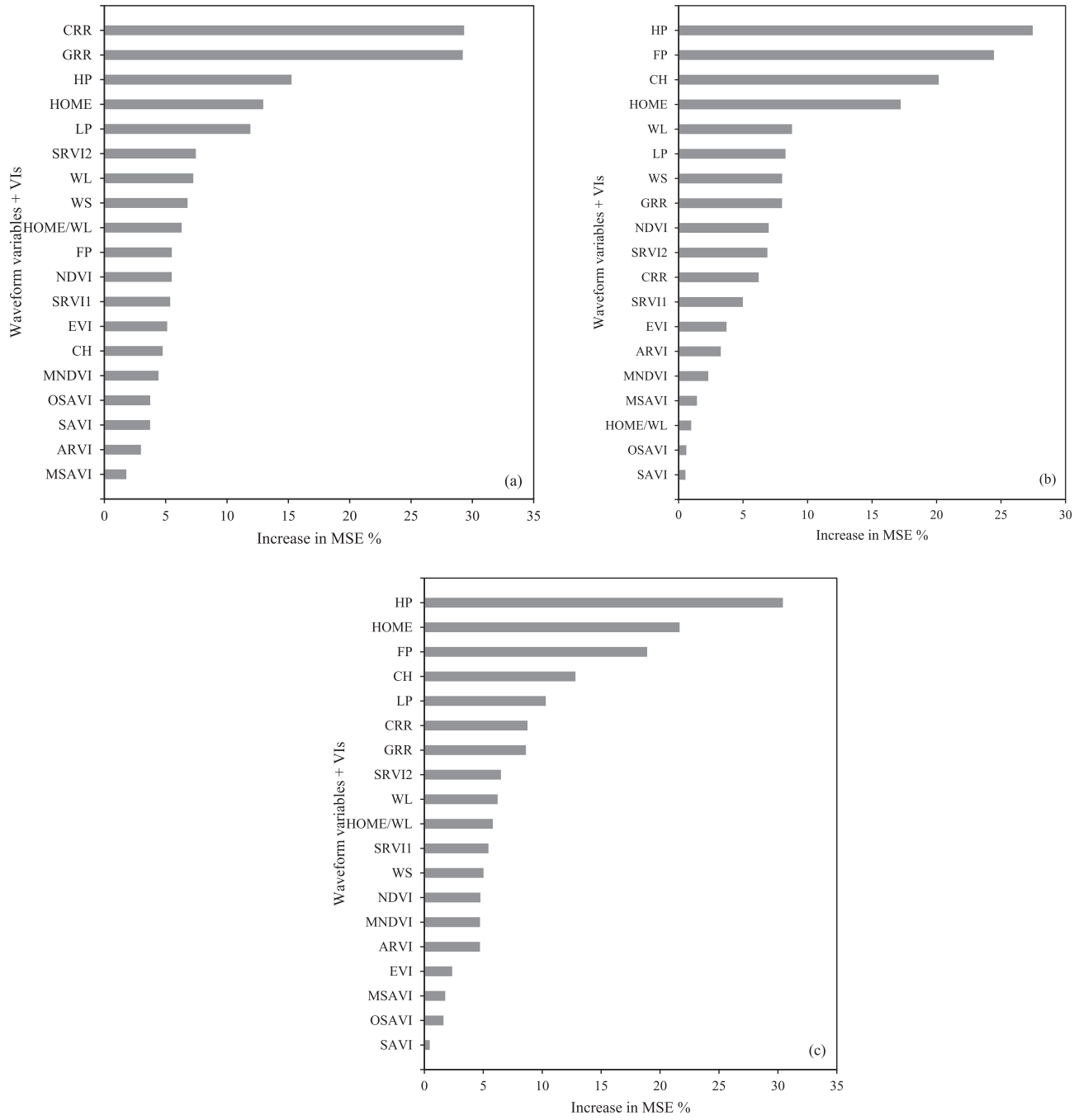

Fig. 6. Variable importance for predicting maize LAI (a), height (b) and biomass (c) by RF regression algorithm using combined VIs and LiDAR pseudo-waveform variables.

waveform and hyperspectral imagery.

In summary, our approach offered the potential for estimating structure parameters of short vegetation, such as crop and herbaceous vegetation. Therefore, in case only discrete-return LiDAR data are available in study area, using pseudo-waveforms to estimate vegetation structure parameters is an alternative method. Although the combination of pseudo-waveforms and hyperspectral imagery improved the estimates of maize LAI, height and biomass, the improvements in precision were small. Thus, there is no need to specifically acquire additional hyperspectral data to improve this small accuracy because additional hyperspectral data signify more cost, especially for large areas and LiDAR data alone can reliably estimate vegetation structure parameters.

Discrete-return LiDAR systems have a dead zone for short vegetation (less than 2 m), however, waveform LiDAR has the potential for providing more accurate data for the dead zone of 2 m. Waveform data can produce more kinds of metrics with low correlation among metrics. In addition, the waveform metrics can provide more physical justification for estimating vegetation structure parameters. Furthermore, when estimating vegetation structure parameters using discrete-return LiDAR data, the height threshold for separating ground returns and vegetation returns should be considered. The height threshold is usually the same value for all plots in the study, which may not be conducive to improving the estimates of vegetation structure parameters, especially for complex terrain. However, for waveform data, we do not need take into account height threshold because the ground can be accurately determined by a waveform decomposition method. Previous studies demonstrate that the sample size of discrete-

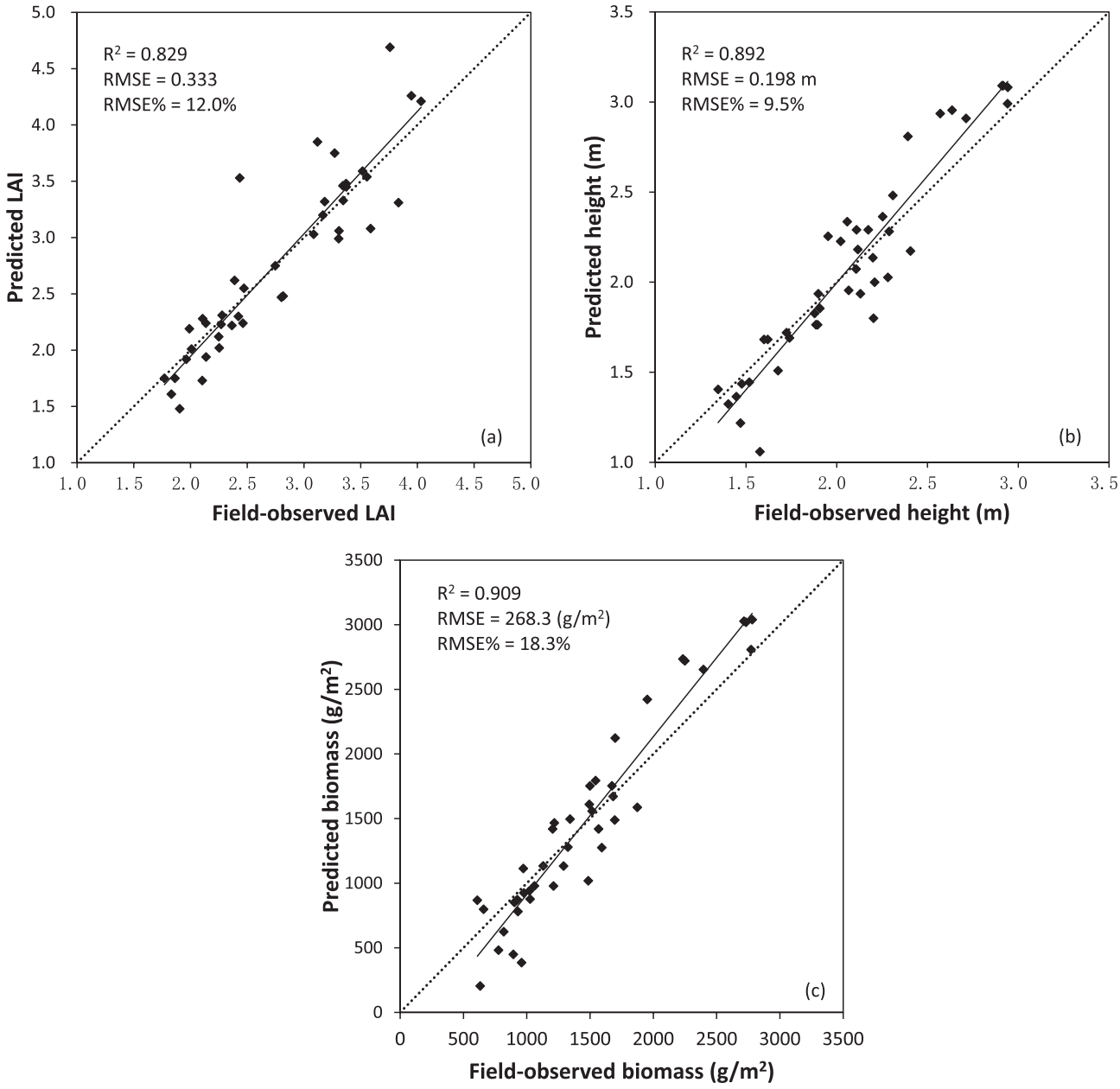

Fig. 7. Scatterplots of field-observed against predicted maize LAI (a), canopy height (b) and above-ground biomass (c) using the combined hyperspectral and pseudo-waveform variables based on RF regression algorithm.

return LiDAR data has an effect on estimation accuracy of vegetation structure parameters (Estornell et al., 2011; Zhao and Popescu, 2009). Similarly, the sample size of pseudo-waveform may affect the estimation accuracy of vegetation structure parameters; however, we did not study the effect of sample size of pseudo-waveform on the estimation accuracy of maize LAI, height and biomass in this study.

5. Conclusions

LiDAR waveform data can provide more vertical profile information of vegetation canopy than discrete-return point clouds. Therefore, the pseudo-waveforms derived from discrete-return LiDAR data have great potential to estimate maize structure parameters. This study presents a useful methodology for estimating maize LAI, height and biomass using combined LiDAR pseudo-waveforms and hyperspectral data. Our results indicate that LiDAR pseudo-waveform variables alone could accurately estimate maize crop LAI, height and biomass. Moreover, the pseudo-waveform variables had a better prediction performance than those traditional statistical variables of discrete-return LiDAR data. However, compared with LiDAR pseudo-waveform variables alone, the combined LiDAR pseudo-waveform variables and VIs improved prediction accuracy of maize LAI, canopy height and AGB. Overall, our study confirms that using the pseudo-waveforms created from discrete-return LiDAR to predict maize structure parameters is a viable method, and the combined pseudo-waveform data and hyperspectral imagery have potential for improving prediction accuracies of crop parameters. Nevertheless, further research is needed to validate our method for predicting LAI, canopy height and AGB with different vegetation types, canopy architectures and plant densities.

Acknowledgments

This research was funded by the National Natural Science Foundation of China (Nos. 41871264 and 41671434). The remotely

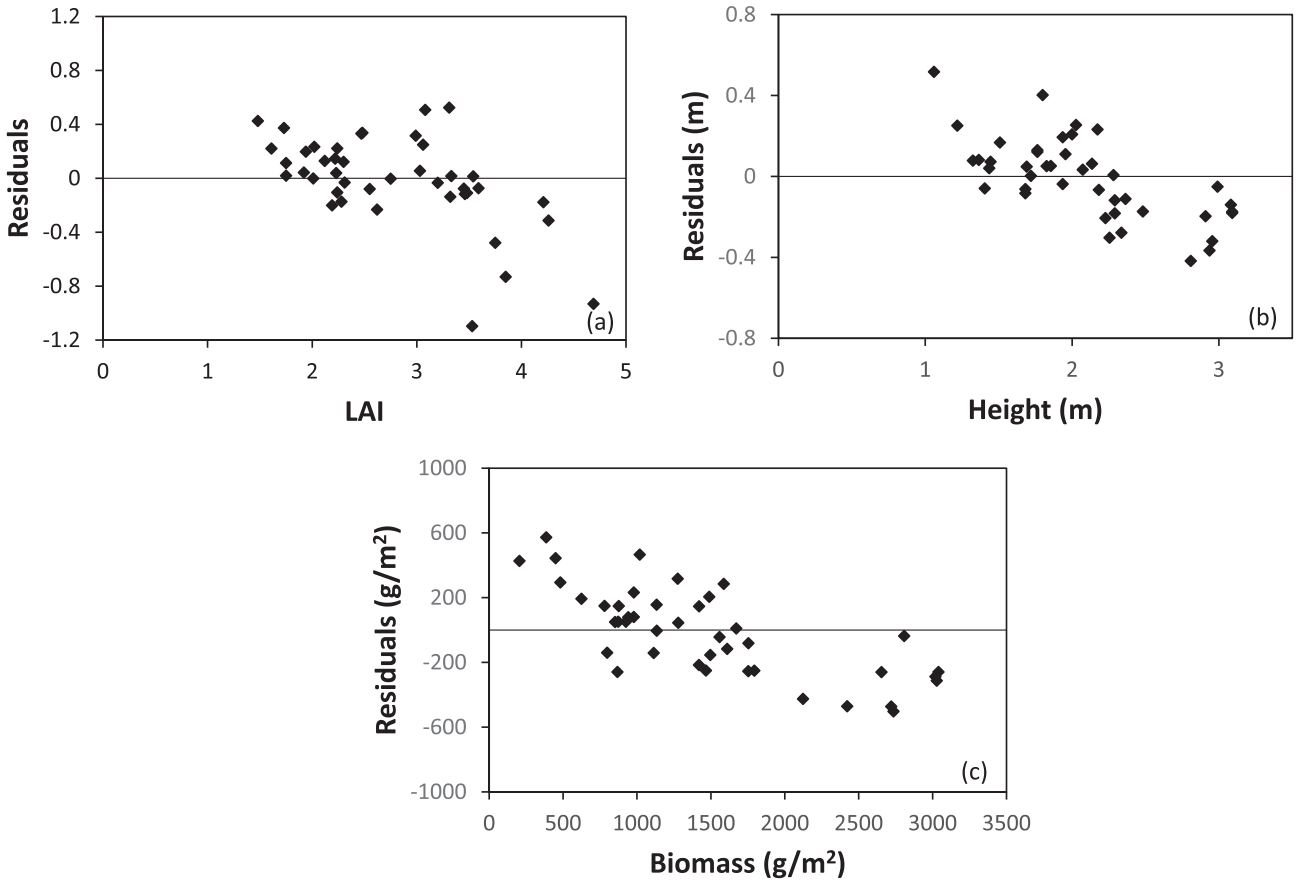

Fig. 8. Residual plots for predicting maize LAI (a), height (b) and biomass (c) using the combined hyperspectral and LiDAR pseudo-waveform variables.

sensed dataset is generated from the "Heihe Watershed Allied Telemetry Experimental Research (HiWATER)". The authors would like to thank the anonymous reviewers for their thoughtful comments and suggestions on the manuscript.

References

Ahmed, R., Siqueira, P., Hensley, S., 2013. A study of forest biomass estimates from lidar in the northern temperate forests of New England. Remote Sens. Environ. 130, 121–135.
Alexander, C., Deák, B., Kania, A., Mücke, W., Heilmeier, H., 2015. Classification of vegetation in an open landscape using full-waveform airborne laser scanner data. Int. J. Appl. Earth Observ. Geoinf. 41, 76–87.
Anderson, K.E., et al., 2018. Estimating vegetation biomass and cover across large plots in shrub and grass dominated drylands using terrestrial lidar and machine learning. Ecol. Indic. 84, 793–802.
Breiman, L., 2001. Random forests. Mach. Learn. 45, 5–32.
Cao, L., Coops, N., Innes, J., Dai, J., She, G., 2014. Mapping above- and below-ground biomass components in subtropical forests using small-footprint LiDAR. Forests 5 (6), 1356.
Chen, J.M., Cihlar, J., 1996. Retrieving leaf area index of boreal conifer forests using Landsat TM images. Remote Sens. Environ. 55 (2), 153–162.
Chen, J.M., Rich, P.M., Gower, S.T., Norman, J.M., Plummer, S., 1997. Leaf area index of boreal forests: theory, techniques, and measurements. J. Geophys. Res. 102 (D24), 29429–29443.
Chen, Q., 2015. Modeling aboveground tree woody biomass using national-scale allometric methods and airborne lidar. ISPRS J. Photogramm. Remote Sens. 106, 95–106.
Chopping, M., et al., 2008. Large area mapping of southwestern forest crown cover, canopy height, and biomass using the NASA multiangle imaging spectro-radiometer. Remote Sens. Environ. 112 (5), 2051–2063.
Clark, M.L., Roberts, D.A., Ewel, J.J., Clark, D.B., 2011. Estimation of tropical rain forest aboveground biomass with small-footprint lidar and hyperspectral sensors. Remote Sens. Environ. 115 (11), 2931–2942.
Dalponte, M., et al., 2018. Predicting stem diameters and aboveground biomass of individual trees using remote sensing data. Ecol. Indic. 85, 367–376.
Drake, J.B., et al., 2002. Estimation of tropical forest structural characteristics using large-footprint lidar. Remote Sens. Environ. 79 (2), 305–319.
Drake, J.B., et al., 2003. Above-ground biomass estimation in closed canopy Neotropical forests using lidar remote sensing: factors affecting the generality of relationships. Global Ecol. Biogeogr. 12 (2), 147–159.
Duncanson, L.I., Niemann, K.O., Wulder, M.A., 2010. Estimating forest canopy height and terrain relief from GLAS waveform metrics. Remote Sens. Environ. 114, 138–154.
Duong, V.H., Lindenbergh, R., Pfeifer, N., Vosselman, G., 2008. Single and two epoch analysis of ICESat full waveform data over forested areas. Int. J. Remote Sens. 29 (5), 1453–1473.
Estornell, J., Ruiz, L.A., Velázquez-Martí, B., Fernández-Sarría, A., 2011. Estimation of shrub biomass by airborne LiDAR data in small forest stands. For. Ecol. Manage. 262 (9), 1697–1703.
Fieber, K.D., et al., 2015. Validation of Canopy Height Profile methodology for small-footprint full-waveform airborne LiDAR data in a discontinuous canopy environment. ISPRS J. Photogramm. Remote Sens. 104, 144–157.
Gao, S., et al., 2015. Height extraction of maize using airborne full-waveform LIDAR data and a deconvolution algorithm. IEEE Geosci. Remote Sens. Lett. 12 (9), 1978–1982.
García, M., Saatchi, S., Ustin, S., Balzter, H., 2018. Modelling forest canopy height by integrating airborne LiDAR samples with satellite Radar and multispectral imagery. Int. J. Appl. Earth Observ. Geoinf. 66, 159–173.
Gleason, C.J., Im, J., 2012. Forest biomass estimation from airborne LiDAR data using machine learning approaches. Remote Sens. Environ. 125, 80–91.
Glenn, N.F., et al., 2011. Errors in LiDAR-derived shrub height and crown area on sloped terrain. J. Arid Environ. 75 (4), 377–382.
Heiskanen, J., Korhonen, L., Hietanen, J., Pellikka, P.K.E., 2015. Use of airborne lidar for estimating canopy gap fraction and leaf area index of tropical montane forests. Int. J. Remote Sens. 36 (10), 2569–2583.
Hermosilla, T., Coops, N.C., Ruiz, L.A., Moskal, L.M., 2014. Deriving pseudo-vertical waveforms from small-footprint full-waveform LiDAR data. Remote Sens. Lett. 5 (4), 332–341.
Hopkinson, C., Chasmer, L., 2009. Testing LiDAR models of fractional cover across multiple forest ecozones. Remote Sens. Environ. 113 (1), 275–288.
Huete, A., Justice, C., Liu, H., 1994. Development of vegetation and soil indices for MODIS-EOS. Remote Sens. Environ. 49 (3), 224–234.
Jakubowski, M.K., Guo, Q., Kelly, M., 2013. Tradeoffs between lidar pulse density and forest measurement accuracy. Remote Sens. Environ. 130, 245–253.
Jonckheere, I., et al., 2004. Review of methods for in situ leaf area index determination. Part I. Theories, sensors and hemispherical photography. Agric. For. Meteorol. 121 (1–2), 19–35.
Jordan, C., 1969. Derivation of leaf-area index from quality of light on the forest floor. Ecology 50 (4), 663–666.
Karna, Y.K., et al., 2015. Integration of WorldView-2 and airborne LiDAR data for tree species level carbon stock mapping in Kayar Khola watershed Nepal. Int. J. Appl. Earth Observ. Geoinf. 38, 280–291.

Kaufman, Y.J., Tanre, D., 1992. Atmospherically resistant vegetation index (ARVI) for EOS-MODIS. IEEE Trans. Geosci. Remote Sens. 30 (2), 261–270.
Kross, A., McNairn, H., Lapen, D., Sunohara, M., Champagne, C., 2015. Assessment of RapidEye vegetation indices for estimation of leaf area index and biomass in corn and soybean crops. Int. J. Appl. Earth Observ. Geoinf. 34, 235–248.
Laurin, V.G., et al., 2014. Above ground biomass estimation in an African tropical forest with lidar and hyperspectral data. ISPRS J. Photogramm. Remote Sens. 89, 49–58.
Li, A., Glenn, N.F., Olsoy, P.J., Mitchell, J.J., Shrestha, R., 2015. Aboveground biomass estimates of sagebrush using terrestrial and airborne LiDAR data in a dryland ecosystem. Agric. For. Meteorol. 213, 138–147.
Li, W., et al., 2016. Generating pseudo large footprint waveforms from small footprint full-waveform airborne LiDAR data for the layered retrieval of LAI in orchards. Opt. Express 24 (9), 10142–10156.
Li, X., et al., 2013. Heihe watershed allied telemetry experimental research (HiWATER): scientific objectives and experimental design. B Am. Meteorol. Soc. 94 (8), 1145–1160.
Liaw, A., Wiener, M., 2002. Classification and regression by random forest. R News 2 (3), 18–22.
Lovell, J.L., Jupp, D.L.B., Culvenor, D.S., Coops, N.C., 2003. Using airborne and ground-based ranging lidar to measure canopy structure in Australian forests. Can. J. Remote Sens. 29 (5), 607–622.
Lu, D., 2006. The potential and challenge of remote sensing-based biomass estimation. Int. J. Remote Sens. 27 (7), 1297–1328.
Lucas, R.M., et al., 2006. Empirical relationships between AIRSAR backscatter and LiDAR-derived forest biomass, Queensland Australia. Remote Sens. Environ. 100 (3), 407–425.
Lucas, R.M., Lee, A.C., Bunting, P.J., 2008. Retrieving forest biomass through integration of CASI and LiDAR data. Int. J. Remote Sens. 29 (5), 1553–1577.
Luo, S., et al., 2018. Comparative performances of airborne LiDAR height and intensity data for leaf area index estimation. IEEE J. Sel. Topics Appl. Earth Observ. Remote Sens. 11 (1), 300–310.
Luo, S., et al., 2016. Effects of LiDAR point density, sampling size and height threshold on estimation accuracy of crop biophysical parameters. Opt. Express 24 (11), 11578–11593.
Luo, S., et al., 2017. Retrieving aboveground biomass of wetland Phragmites australis (common reed) using a combination of airborne discrete-return LiDAR and hyperspectral data. Int. J. Appl. Earth Observ. Geoinf. 58, 107–117.
Ma, H., Song, J., Wang, J., Xiao, Z., Fu, Z., 2014. Improvement of spatially continuous forest LAI retrieval by integration of discrete airborne LiDAR and remote sensing multi-angle optical data. Agric. For. Meteorol. 189–190, 60–70.
Ma, Q., et al., 2018. Evaluating the uncertainty of Landsat-derived vegetation indices in quantifying forest fuel treatments using bi-temporal LiDAR data. Ecol. Indic. 95, 298–310.
Magruder, L.A., 2010. Lidar waveform stacking techniques for faint ground return extraction. J. Appl. Remote Sens. 4 (1).
Mesas-Carrascosa, F.J., Castillejo-González, I.L., de la Orden, M.S., Porras, A.G.-F., 2012. Combining LiDAR intensity with aerial camera data to discriminate agricultural land uses. Comput. Electron. Agric. 84, 36–46.
Mielcarek, M., Stereńczak, K., Khosravipour, A., 2018. Testing and evaluating different LiDAR-derived canopy height model generation methods for tree height estimation. Int. J. Appl. Earth Observ. Geoinf. 71, 132–143.
Moeser, D., Roubinek, J., Schleppi, P., Morsdorf, F., Jonas, T., 2014. Canopy closure, LAI and radiation transfer from airborne LiDAR synthetic images. Agric. For. Meteorol. 197, 158–168.
Muss, J.D., Mladenoff, D.J., Townsend, P.A., 2011. A pseudo-waveform technique to assess forest structure using discrete lidar data. Remote Sens. Environ. 115 (3), 824–835.
Mutanga, O., Skidmore, A.K., 2004. Narrow band vegetation indices overcome the saturation problem in biomass estimation. Int. J. Remote Sens. 25 (19), 3999–4014.
Nie, S., Wang, C., Zeng, H., Xi, X., Li, G., 2017. Above-ground biomass estimation using airborne discrete-return and full-waveform LiDAR data in a coniferous forest. Ecol. Indic. 78, 221–228.
Nie, S., Wang, C., Zeng, H., Xi, X., Xia, S., 2015. A revised terrain correction method for forest canopy height estimation using ICESat/GLAS data. ISPRS J. Photogramm. Remote Sens. 108, 183–190.
Pang, Y., Lefsky, M., Sun, G., Ranson, J., 2011. Impact of footprint diameter and off-nadir pointing on the precision of canopy height estimates from spaceborne lidar. Remote Sens. Environ. 115 (11), 2798–2809.
Phua, M.-H., et al., 2017. Synergistic use of Landsat 8 OLI image and airborne LiDAR data for above-ground biomass estimation in tropical lowland rainforests. For. Ecol. Manage. 406, 163–171.
Pirotti, F., Laurin, G., Vettore, A., Masiero, A., Valentini, R., 2014. Small footprint full-waveform metrics contribution to the prediction of biomass in tropical forests. Remote Sens. 6 (10), 9576–9599.
Popescu, S.C., Zhao, K., 2008. A voxel-based lidar method for estimating crown base height for deciduous and pine trees. Remote Sens. Environ. 112 (3), 767–781.
Popescu, S.C., Zhao, K., Neuenschwander, A., Lin, C., 2011. Satellite lidar vs. small footprint airborne lidar: comparing the accuracy of aboveground biomass estimates and forest structure metrics at footprint level. Remote Sens. Environ. 115 (11), 2786–2797.
Qi, J., Chehbouni, A., Huete, A.R., Kerr, Y.H., Sorooshian, S., 1994. A modified soil adjusted vegetation index. Remote Sens. Environ. 48 (2), 119–126.
Qin, Y., Li, S., Vu, T.-T., Niu, Z., Ban, Y., 2015. Synergistic application of geometric and radiometric features of LiDAR data for urban land cover mapping. Opt. Express 23 (11), 13761–13775.
Riaño, D., Valladares, F., Condés, S., Chuvieco, E., 2004. Estimation of leaf area index and covered ground from airborne laser scanner (Lidar) in two contrasting forests. Agric. For. Meteorol. 124 (3–4), 269–275.
Richardson, J.J., Moskal, L.M., Kim, S.-H., 2009. Modeling approaches to estimate effective leaf area index from aerial discrete-return LIDAR. Agric. For. Meteorol. 149 (6–7), 1152–1160.
Rondeaux, G., Steven, M., Baret, F., 1996. Optimization of soil-adjusted vegetation indices. Remote Sens. Environ. 55 (2), 95–107.
Rouse, J.W., Haas, R.H., Schell, J.A. and Deering, D.W., 1973. Monitoring vegetation systems in the Great Plains with ERTS. Third Earth Resources Technology Satellite-1 Symposium: pp. 309–317.
Silva, C.A., et al., 2018. Comparison of small- and large-footprint lidar characterization of tropical forest aboveground structure and biomass: a case study from central gabon. IEEE J. Sel. Topics Appl. Earth Observ. Remote Sens. 1–15.
Swatantran, A., Dubayah, R., Roberts, D., Hofton, M., Blair, J.B., 2011. Mapping biomass and stress in the Sierra Nevada using lidar and hyperspectral data fusion. Remote Sens. Environ. 115 (11), 2917–2930.
Takagi, K., et al., 2015. Forest biomass and volume estimation using airborne LiDAR in a cool-temperate forest of northern Hokkaido, Japan. Ecol. Inform. 26, 54–60.
Tao, S., et al., 2014. Airborne Lidar-derived volume metrics for aboveground biomass estimation: a comparative assessment for conifer stands. Agric. For. Meteorol. 198–199, 24–32.
Tesfamichael, S.G., van Aardt, J., Roberts, W., Ahmed, F., 2018. Retrieval of narrow-range LAI of at multiple lidar point densities: application on Eucalyptus grandis plantation. Int. J. Appl. Earth Observ. Geoinf. 70, 93–104.
Tian, J., Wang, L., Li, X., 2015. Sub-footprint analysis to uncover tree height variation using ICESat/GLAS. Int. J. Appl. Earth Observ. Geoinf. 35, 284–293.
Varvia, P., Rautiainen, M., Seppänen, A., 2018. Bayesian estimation of seasonal course of canopy leaf area index from hyperspectral satellite data. J. Quant. Spectrosc. Radiat. Transfer 208, 19–28.
Wagner, W., Ullrich, A., Ducic, V., Melzer, T., Studnicka, N., 2006. Gaussian decomposition and calibration of a novel small-footprint full-waveform digitising airborne laser scanner. ISPRS J. Photogramm. Remote Sens. 60 (2), 100–112.
Xi, X., et al., 2016. Forest above ground biomass inversion by fusing GLAS with optical remote sensing data. ISPRS Int. J. Geo-Inf. 5 (4), 45.
Xiao, Q. and Wen, J., 2013. HiWATER: Airborne LiDAR-DSM data production in the middle reaches of the Heihe River Basin. Cold and Arid Regions Science Data Center at Lanzhou.
Zhao, F., Guo, Q., Kelly, M., 2012. Allometric equation choice impacts lidar-based forest biomass estimates: a case study from the Sierra National Forest, CA. Agric. For. Meteorol. 165, 64–72.
Zhao, K., Popescu, S., 2009. Lidar-based mapping of leaf area index and its use for validating GLOBCARBON satellite LAI product in a temperate forest of the southern USA. Remote Sens. Environ. 113 (8), 1628–1645.
Zheng, G., et al., 2017. Retrieving directional gap fraction, extinction coefficient, and effective leaf area index by incorporating scan angle information from discrete aerial lidar data. IEEE Trans. Geosci. Remote Sens. 55 (1), 577–590.
Zhou, Y., Qiu, F., 2015. Fusion of high spatial resolution Worldview-2 imagery and LiDAR pseudo-waveform for object-based image analysis. ISPRS J. Photogramm. Remote Sens. 101, 221–232.
Zolkos, S.G., Goetz, S.J., Dubayah, R., 2013. A meta-analysis of terrestrial aboveground biomass estimation using lidar remote sensing. Remote Sens. Environ. 128, 289–298.